scientific reports

Check for updates

OPEN

Design of a compact quasi-optical mode converter for a 105-GHz gyrotron using optimized perturbation technique

Hamid Sharif[1]✉, Muhammad Haris Jamil[1], Nazish Saleem Abbas[2] & Wenlong He[1]✉

This paper presents the design and optimization of a compact quasi-optical (QO) mode converter for a high-performance gyrotron operating at 105 GHz in the $TE_{17,6}$ mode. The converter integrates a dimpled-wall launcher with a novel dual-direction perturbation technique alternating positive and negative deviations based on coupled mode theory. This approach reduces the launcher length to 85 mm, with a cut length of 20 mm (23.53% of the total length), while maintaining high mode conversion efficiency. MATLAB-based parametric analysis was used to optimize the launcher's field distribution, and FEKO simulations validated its radiation performance. The mirror system comprising quasi-elliptical, elliptical, and parabolic mirrors ensures precise phase correction and beam shaping, contributing to high mode purity and compactness. Simulations demonstrate outstanding performance, achieving 99.4% scalar and 98.6% vector Gaussian mode content at the output. This design offers a compact and efficient solution for next-generation millimeter-wave applications.

Keywords Quasi-optical mode converter, Denisov-launcher, Gyrotron, Terahertz

Modern gyrotrons, capable of delivering up to 1 MW of continuous-wave radiation in the millimeter and terahertz ranges, are vital for applications such as ECRH and ECCD in fusion reactors like ITER and Wendelstein 7-X, as well as plasma diagnostics and industrial processing[1–5]. Gyrotrons operate in high-order transverse electric (TE) modes, which need to be converted into Gaussian beams to ensure efficient transmission, precise focusing, and minimal losses. This conversion is achieved through quasi-optical mode converters (QOMCs), which minimize stray radiation, ensure high efficiency, and support stable continuous-wave (CW) operation in high-power systems[6–11]. QOMCs comprise a launcher that transforms the cavity mode into a Gaussian-like beam and a mirror system that reshapes its phase. High conversion efficiency is critical not only for reducing power losses but also for ensuring reliable, long-term gyrotron operation[12–15].

Denisov-type launchers[16–21], commonly used in modern gyrotron designs, employ strategic perturbations that reshape the inner surface to guide high-order TE modes into a focused Gaussian beam profile while minimizing edge diffraction at the launcher aperture. This results in an astigmatic Gaussian-like radiation pattern. Coupled-mode theory decomposes the initial cavity mode into multiple components, enabling a gradual transformation into a Gaussian-like field distribution along the waveguide wall. The mirror system then transforms the astigmatic Gaussian-like beam into the fundamental Gaussian mode (TEM 00), ensuring high beam quality, minimal diffraction losses, and optimal mode conversion efficiency.

The length of the quasi-optical launcher is a critical design parameter that directly influences the interaction between the electron beam and the RF wave, thereby affecting mode conversion efficiency and beam quality. A compact launcher reduces undesired mode competition, diffraction losses, wave reflections, and energy dissipation. It also lowers the risk of mechanical deformations and alignment errors during manufacturing, ensuring greater precision and operational stability. The presence of the electron beam imposes strict design requirements, as imperfections can lead to spurious oscillations or mode mismatches. Although the total system length is constrained by the need to clear the superconducting magnet, optimizing the launcher length independently improves efficiency, thermal management, and system integration[22,23].

These advantages highlight the importance of launcher length optimization in designing space-efficient, high-performance QOMCs for millimeter-wave applications. However, designing compact and efficient QOMCs

[1]College of Electronics and Information Engineering, Shenzhen University, 3688, Shenzhen, Guangdong 518060, China. [2]College of Physics and Optoelectronic, Shenzhen University, 3688, Shenzhen, Guangdong 518060, China. ✉email: hamidnumls@gmail.com; wenlong.he@szu.edu.cn

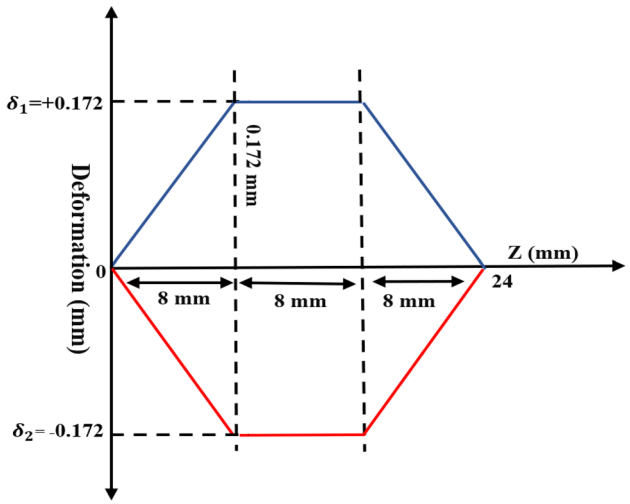

Fig. 1. Deformation profile of the launcher wall with dual-direction perturbations (δ_1 = +0.172 mm, δ_2 = −0.172 mm) superimposed on the mean radius (R_0 = 19 mm). The amplitudes over 24 mm along z, providing both axial and radial variation of the inner-wall perturbations.

Ref	Freq. (GHz)	Mode	Length (mm)	Cut (mm)	Gaussian (%)	Eff. (%)
[11]	104.9	$TE_{17,6}$	168	43.4	95.2%	96.9%
[24]	105	$TE_{17,6}$	170	40	99.09%	NA
[25]	105/140	$TE_{18,7}/TE_{24,9}$	150	42	98% for 105 GHz 99.7% for 140 GHz	97.3% for 105 GHz 99.0% for 140 GHz
[26]	105/140	$TE_{17,6}/TE_{22,8}$	183	68	94%–98%	90%
[27]	104.9–143.3	Multi-mode (Optimize at $TE_{17,6}$ and 104.9 GHz)	160	40	∼98.0% at $TE_{17,6}$ for 104.9 GHz	NA
[28]	104.9–143	Multi-mode (Optimize at $TE_{17,6}$ and 104.9 GHz)	168	50	95.2% at $TE_{17,6}$ for 104.9 GHz	96.9% at $TE_{17,6}$ for 104.9 GHz
This work	**105**	**$TE_{17,6}$**	**85**	**20 (23.53% of total length)**	98.6% (vector) 99.4% (scalar)	**98.6%**

Table 1. Comparison of quasi-optical mode converter designs for gyrotron systems, highlighting launcher length, cut length, Gaussian mode content, and conversion efficiency.

presents key challenges, particularly in achieving optimal beam quality and conversion performance within tight space constraints. Accurate propagation distances are essential for phase matching among modes to achieve a Gaussian-like field profile at the output. For high-order modes, the launcher must be sufficiently long to allow full field development, and this length is strongly influenced by the launcher radius. While theoretical models provide an initial estimate, empirical adjustments are often required. In general, launcher length is proportional to radius and varies with mode type and wavelength. A radius that is too small leads to excessive diffraction and reduced efficiency, while a larger radius may necessitate a longer launcher to prevent edge reflections. Balancing these parameters is critical for minimizing losses and achieving effective mode conversion. Perturbation amplitude and length are key design parameters that affect launcher size, beam stability, and field distribution. Fine-tuning these values enables precise control over mode conversion and phase matching, facilitating a compact yet highly efficient design. When optimized, these perturbations allow for shorter launcher lengths while maintaining high mode purity and minimizing reflections.

Unlike conventional designs that apply unidirectional perturbations, this study introduces a dual-direction technique using alternating positive and negative deviations. This approach enhances control over field shaping and mode conversion, enabling a more compact and efficient launcher. Specifically, symmetrical deviations of δ_1 = +0.172 mm and δ_2 = -0.172 mm are applied along the launcher wall, as shown in the deformation profile (Fig. 1). This balanced perturbation reshapes the electromagnetic field, enhancing mode purity, reducing reflections, and ensuring a smooth field transition that enables the transformation of the complex TE mode into a Gaussian-like beam. By optimizing the perturbation parameters, the launcher length is reduced to 85 mm without sacrificing conversion efficiency. This technique effectively addresses the challenges of achieving both compactness and high performance, offering substantial improvements over existing designs.

Various studies have proposed methods to enhance the performance of quasi-optical mode converters (QOMCs), with particular emphasis on parameters such as launcher length, cut length, and conversion efficiency. To place our results in context, Table 1 provides a summary of recent QOMC designs, outlining key characteristics including launcher length, cut length, Gaussian mode content, and overall efficiency. In

comparison, the proposed QOMC demonstrates notable improvements in both compactness and performance, featuring a launcher length of 85 mm, scalar Gaussian mode content of 99.4%, and vector Gaussian mode content of 98.6%.

The QOMC system consists of a precisely engineered launcher and an optimized mirror assembly. Initial dimensional parameters of the launcher were calculated using geometric optics principles in MATLAB R2021b. These parameters were then used in the FEKO simulation tool (Altair Simulation Products Version 2021.1) to model the electromagnetic field distribution around the cylindrical launcher and at the output window. The design was validated and further refined through FEKO simulations, which guided additional optimization to enhance mode purity and reduce diffraction losses. The proposed mirror system comprises a quasi-elliptical mirror, an elliptical mirror, and a parabolic phase-correction mirror, forming a compact and efficient configuration. With phase correction applied, the system achieves a scalar Gaussian mode content of 99.4% and a vector Gaussian mode content of 98.6% at 105 GHz. These results confirm the effectiveness of the complete QOMC in delivering high mode conversion efficiency. Compared to other designs operating at the same frequency, the proposed system demonstrates superior performance in terms of both mode purity and compactness. The integration of reduced launcher and cut lengths with the dual-direction perturbation and phase-compensation techniques leads to a more space-efficient and high-performing design.

The remainder of this paper is structured as follows: Section II outlines the launcher design, Section III presents the mirror configuration, Section IV details simulation results and performance analysis, and Section V concludes the study.

Launcher design with dual-direction perturbation

Quasi-optical mode converters (QOMCs) employ a periodic helical Denisov launcher with precisely engineered perturbations to alter the boundary conditions of the waveguide's inner wall. This modification enables the coupling of the input eigenmode of the circular waveguide with other modes, as described by coupled mode theory. A raised-cosine tapered field distribution, resembling an astigmatic Gaussian beam, is utilized to establish the selection rules for the perturbations[29].

$$\Delta\beta = \pm\frac{2\pi}{L_c}, \quad \Delta m = \pm\frac{\pi}{\theta}, \quad \cos\theta = \frac{m}{X_{mn}}, \quad \theta = \arccos\left(\frac{m}{X_{mn}}\right) \tag{1}$$

Here "m" represents the azimuthal mode index, while "n" represents the radial mode index. X_{mn} corresponds to the root of the Bessel function (or its derivative), L_c represents the cut length of the launcher, R_c and 'R_0' represent the caustic radius and cavity radius, respectively. The transverse reflection angle θ is shown in Fig. 2. The radial variation along the launcher wall is defined by the expression[23]:

$$R(\phi, z) = R_0 + \alpha z + \delta_1(z)\cos\left(\Delta\beta_1 z - l_1\phi\right) + \delta_2(z)\cos\left(\Delta\beta_2 z - l_2\phi\right) \tag{2}$$

In this analysis, the initial radius of the launcher is represented by R_0, while α denotes the taper slope of the wall radius. The longitudinal position is indicated by z, and the azimuthal angle is represented by ϕ. The perturbation amplitudes in the longitudinal and azimuthal directions are denoted by δ_1 and δ_2, respectively, as illustrated in the schematic deformation profile (Fig. 1). In this context, β_1 is defined as half of the difference in the longitudinal wavenumber associated with the longitudinal coupling modes, while β_2 refers to half of the difference in the longitudinal wavenumber for the azimuthal coupling modes. Additionally, l_1 and l_2 represent the periods of azimuthal perturbation in both the longitudinal and azimuthal components, respectively. Here l_1,l_2,$\Delta\beta_1$, $\Delta\beta_2$ is defined as:

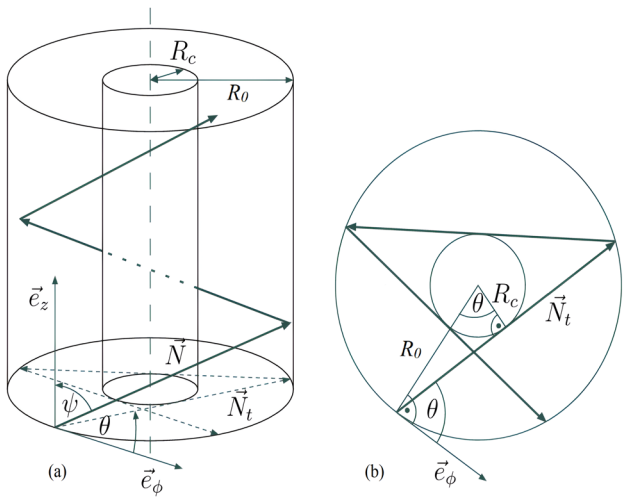

Fig. 2. Geometric optical representation of ray path in cylindrical waveguide: (**a**) side view; (**b**) top view.

$$l_1 = \pm(m_1 - m_2) = \pm 1 \tag{3}$$

$$l_2 = \pm(m_1 - m_2) = \pm 3 \tag{4}$$

$$\Delta\beta_1 = \frac{1}{2}(\beta_{m-1,n} - \beta_{m+1,n}) = \frac{1}{2}\left[\sqrt{k_0^2 - \left(\frac{X_{m-1,n}}{R_0 + \alpha z}\right)^2} - \sqrt{k_0^2 - \left(\frac{X_{m+1,n}}{R_0 + \alpha z}\right)^2}\right] \tag{5}$$

$$\Delta\beta_2 = \frac{1}{2}(\beta_{m-\Delta m,n+\Delta n} - \beta_{m+\Delta m,n-\Delta n}) = \frac{1}{2}\left[\sqrt{k_0^2 - \left(\frac{X_{m-\Delta m,n+\Delta n}}{R_0 + \alpha z}\right)^2} - \sqrt{k_0^2 - \left(\frac{X_{m+\Delta m,n-\Delta n}}{R_0 + \alpha z}\right)^2}\right] \tag{6}$$

Coupled mode theory effectively analyzes wave propagation in waveguides with minor surface irregularities, facilitating the evaluation of the interaction between the principal mode and satellite modes in response to variations in wall perturbations.

Typically, the equations that characterize the coupling between forward-propagating waves are expressed as follows:

$$(dA_i)/dz = -j\beta_i A_i + \sum_k C_{ip} A_k \tag{7}$$

Only the *TE* mode is considered, with the coefficient C_{ip} described in[30].

$$C_{ip} = \frac{j\delta}{2R\sqrt{k_{zi}k_{zp}}\sqrt{(x'^2_{m1p1} - m_1^2)(x'^2_{m2p2} - m_2^2)}} \times \left[\frac{x'^2_{m1p1}}{R^2}(x'^2_{m1p1} - m_1 m_2) \pm \Delta\beta k_{zp}\epsilon m_1 m_2\right] \exp(\pm\Delta\beta z) \tag{8}$$

where X_{mp} is the root of Bessel function's derivate.

The design procedure for the launcher is performed in two steps. Firstly, the irregular waveguide mode converter is analyzed by using coupled mode theory. Secondly, the radiated fields are calculated from the waveguide cut using the vector diffraction integral.

In the design of quasi-optical launchers, the perturbation amplitude and launcher radius are key parameters, which have significant effects on the overall size and performance of the launcher. If the perturbation length is too small, the process of mode conversion is not complete, resulting in mode mismatches and low conversion efficiency. Conversely, if the perturbation length is too large, it can result in too much phase shifts, causing unwanted mode generation and higher diffraction losses. Similarly, the launcher radius is essential to diffraction control and mode confinement. Large mode coupling and diffraction occur with a small radius, lowering mode purity and raising reflection losses. Conversely, an increasing radius requires more gradual tapering, leading to a longer launcher, increasing interaction length and the likelihood of undesirable mode competition. By precisely adjusting perturbation length and launcher radius, our design achieves high mode purity and compact, efficient mode conversion. This delicate balance doesn't just limit energy loss, but it also maximizes system stability and performance.

This work introduces a novel perturbation technique that applies both positive and negative amplitude variations relative to the mean radius, in contrast to previous studies that employed exclusively positive values. The launcher has a mean radius of 19 mm, with two helical wall perturbations of amplitudes δ_1 = +0.172 mm and δ_2 = –0.172 mm applied relative to this mean radius. These perturbations are confined to an axial region of 24 mm (from z = 0 mm to z = 24 mm), while the launcher wall remains unperturbed outside this range. This configuration achieves an optimal balance between perturbation length and field control, resulting in a significantly reduced launcher length of 85 mm. The perturbation profile is illustrated in Fig. 1.

The carefully tailored perturbations gradually shape the electromagnetic field distribution, ensuring that the required amplitude and phase relationships for efficient mode conversion are maintained. The strategic incorporation of both positive and negative perturbations not only minimizes energy losses but also enhances mode purity, resulting in a compact launcher design that optimizes performance while reducing overall size. All parameters were derived using MATLAB R2021b and subsequently used to construct and simulate the launcher in the FEKO simulation tool (Altair Simulation Products Version 2021.1).

Theoretically, a sudden alteration in the waveguide's shape can couple an infinite number of modes. However, given the minimal perturbation amplitude of the Denisov launcher, only eight primary coupling modes are taken into account. Additionally, the relative power of nine modes is evaluated based on the results of the Gaussian mode decomposition, as outlined in Table 2. The waveguide mode converter is analyzed using coupled mode theory, and the radiated fields are computed through the vector diffraction integral of the waveguide cross-section.

Figure 3 illustrates the evolution of modal power along the launcher length, confirming the coupling behavior and development of the Gaussian profile for the helical mode converter operating at 105 GHz using the $TE_{17,6}$ mode. In Fig. 3, the graph illustrates the evolution of mode distribution along the converter's length. Initially, at $z = 0$, where the wall variation begins, a pure rotating $TE_{17,6}$ mode is introduced. As the radiation propagates along the z-axis, power in the $TE_{17,6}$ mode progressively couples by using couple mode theory into eight satellite modes primarily influenced by wall perturbations. Notably, significant couplings originate from the $TE_{17,6}$ mode to four satellite modes: $TE_{18,6}$, $TE_{16,6}$, $TE_{20,5}$, and $TE_{14,7}$. The analysis also takes into account additional modes that couple with the $TE_{17,6}$, mode due to deformations in the waveguide wall. These modes

	Azimuthal bunching →		
Axial bunching →	$TE_{15,7}$ (3%)	$TE_{18,6}$ (11%)	$TE_{21,5}$ (3%)
	$TE_{14,7}$ (11%)	$TE_{17,6}$ (44%)	$TE_{20,5}$ (11%)
	$TE_{13,7}$ (3%)	$TE_{16,6}$ (11%)	$TE_{19,5}$ (3%)

Table 2. A set of TE modes is employed to generate a Gaussian-like field distribution characterized by relative power.

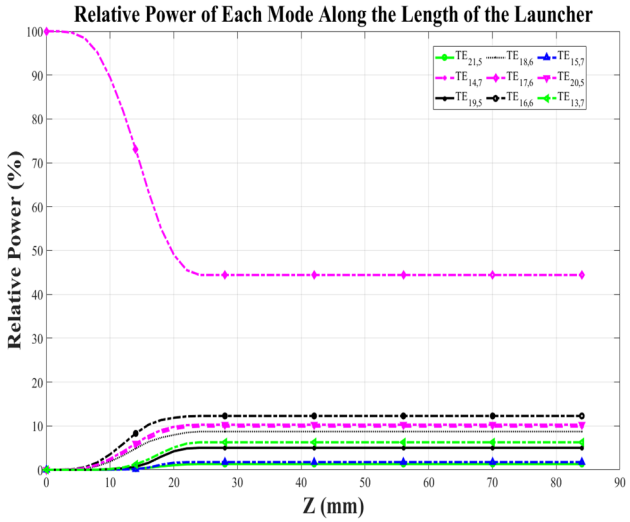

Fig. 3. Evolution of relative power coefficients for the primary and satellite modes along the z-axis.

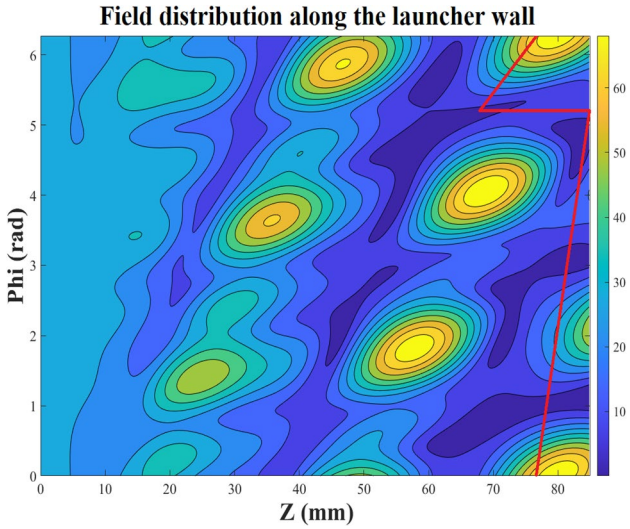

Fig. 4. Electric field distribution along the z-axis (MATLAB).

play a significant role in enhancing the peak amplitude of the Gaussian field distribution while simultaneously lowering the sidelobe power levels.

The waveguide wall current distribution in the Denisov launcher shows that the beam is effectively focused, resulting in high fundamental Gaussian beam content at the launcher aperture. Figure 4 shows the Electric field amplitude distribution (in dB) on the unfolded inner surface of the tapered launcher. The solid line indicates the helical cut, located at 4.886 rad, beginning at $z = 65$ mm, with a cut length of 20 mm. Figure 5 highlights that although the phase of each mode starts at zero, it evolves along the z-axis due to periodic perturbations. These perturbations bring the phases of each mode nearly into alignment by the aperture, contributing to a high

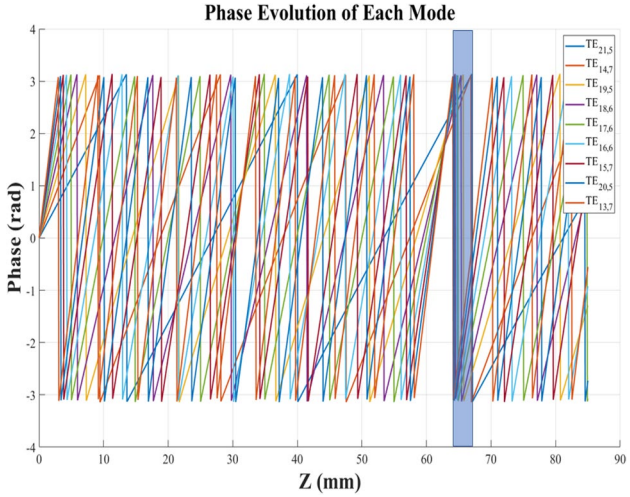

Fig. 5. Phase distribution of each mode along the z-axis.

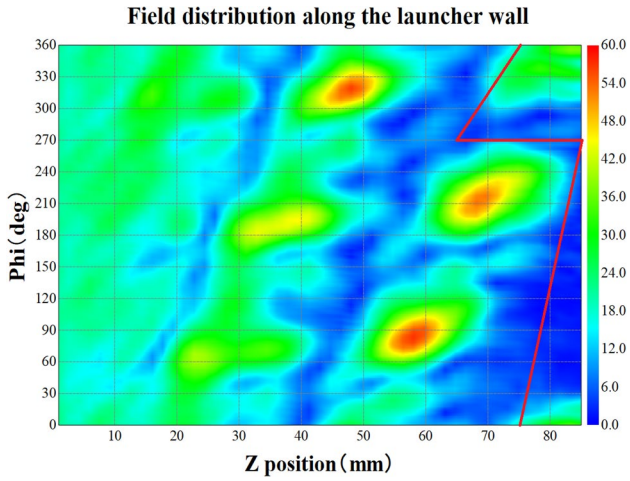

Fig. 6. Electric field distribution along the z-axis (FEKO simulation).

fundamental Gaussian mode content (FGMC) and Fig. 6 shows the field distribution simulated using FEKO (contour graph). The results illustrate that the $TE_{17,6}$ mode fed into the waveguide gradually evolves into a high-quality Gaussian beam spot after the structured perturbations on the inner wall of the waveguide. This transformation facilitates efficient wave energy radiation and transfer. In this study, we achieved efficient mode conversion using a compact QO launcher with a length of 85 mm and a radius of 19 mm for the $TE_{17,6}$ mode at 105 GHz. This was accomplished through the careful optimization of launcher radius, perturbation amplitude, and perturbation length. By precisely fine-tuning these parameters, we enhanced the launcher's ability to guide and shape the electromagnetic field, ensuring high mode purity and minimal energy losses while maintaining a reduced propagation distance.

To achieve this Gaussian output pattern, specific relationships involving the amplitude and phase of the primary mode relative to the satellite modes are required. This precise shaping ensures efficient energy radiation toward the mirror system, forming the basis for the subsequent quasi-optical transformation.

Mirror system configuration:

The quasi-optical mode converter (QOMC) integrates a Denisov-type launcher with a precisely engineered mirror system to convert the high-order cavity mode ($TE_{17,6}$ at 105 GHz) into a fundamental Gaussian beam. This transformation addresses the deviation between the launcher's emitted field and the ideal Gaussian profile, enabling efficient transmission and high-quality beam focusing.

The mirror system, consisting of a quasi-elliptical mirror, an elliptical mirror, and a phase-correction parabolic mirror, is strategically designed to guide the electromagnetic beam and produce a well-defined field distribution at the gyrotron output window. The optical path configuration of this QOMC is illustrated in Fig. 7, showcasing the arrangement of the three mirrors optimized for compactness and high conversion efficiency.

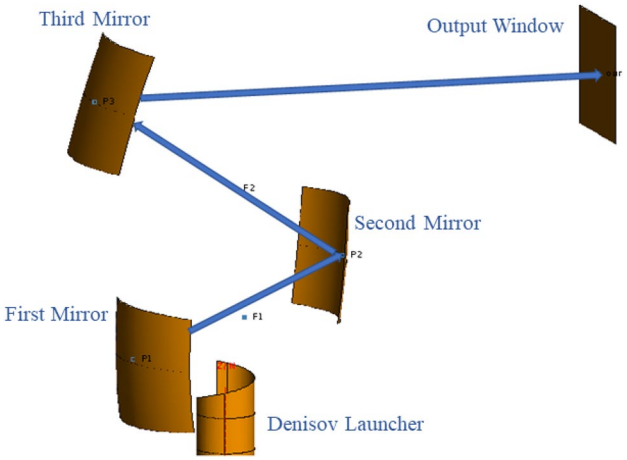

Fig. 7. Optical path layout of the converter system.

The beam-shaping process relies on three reflective surfaces, each playing a distinct role in achieving the desired beam structure:

First mirror (quasi-elliptical mirror)

The first-stage mirror is designed with a quasi-elliptical shape to facilitate horizontal beam re-convergence. Its secondary focus (F_1) is positioned close to the z-axis, reducing the lateral dimensions of the mirror while maintaining effective focusing.

The parameters for the first-stage mirror are obtained by deriving the surface coordinates from Eq. (9), which is inserted into Eqs. (10) and (11). This allows accurate calculation of the quasi-elliptical mirror's surface profile[23].

$$l(\phi) = \frac{8R_c l_2 \cos\phi - 4\phi^2 R_c^2 - 4\phi R_c^2 \pi + 8\phi R_c l_g - \pi^2 R_c^2 + 4\pi R_c l_g + 8l_1 l_g - 8l_1 l_2}{8l_2 \sin\phi + 8\phi R_c + 4\pi R_c + 8l_g} \tag{9}$$

$$x(\phi) = R_c \cos\phi + l(\phi)\sin\phi \tag{10}$$

$$y(\phi) = R_c \sin\phi + l(\phi)\cos\phi \tag{11}$$

These equations enable precise optimization of the mirror's surface geometry, ensuring accurate horizontal re-convergence of the beam. The position of the first mirror is defined as $(x, y, z) = (40, 0, 105)$, with its secondary focus (F_1) located at (10, 0, 125).

Second mirror (elliptical mirror)

The second-stage mirror, is an elliptical in shape, continues the horizontal beam re-convergence process. Its primary focal point aligns with the secondary focus (F_1) of the first-stage mirror, while its secondary focus is positioned at the distant output window. Additionally, this mirror functions as a zoom lens, allowing adjustable focal length variations along the z-axis. This flexibility ensures optimal beam shaping and alignment, adapting to the specific requirements of the system. The position of the second mirror is defined as $(x, y, z) = (-75, 0, 163.5954)$.

Third mirror (parabolic mirror)

The third-stage mirror maintains a parabolic configuration to achieve vertical beam convergence. It directs the beam toward the center of the output window, ensuring precise vertical focusing and symmetry in the final Gaussian beam. This stage is critical for producing a well-collimated and symmetric output beam. The position of the third mirror is defined as $(x, y, z) = (139.19, 0, 325)$. The output window, where the final Gaussian beam is formed, is located at $(x, y, z) = (-140, 0, 325)$. Furthermore, in subsequent designs, the third-level mirror will incorporate a phase correction surface functionality.

Results and analysis

A comprehensive analysis of beam convergence was conducted using full-wave electromagnetic modeling, based on the established radiation field distribution. The evaluation began with the source field emitted by the launcher, followed by the computation of the reflected field at the first mirror surface and the incident field on the second mirror, enabling precise tracking of the beam's evolution through the system. The field exiting the second mirror was subsequently analyzed, and the reflected field from the third mirror was determined. Finally, the resulting field distribution at the output window, presented in Fig. 8, confirms effective beam convergence and the formation of a well-defined beam waist. The fitted Gaussian parameters indicate a beam waist of w_0 = 8.8 mm ($\approx 3.08\lambda$) located at the output window, with the corresponding phase distribution shown in Fig. 9.

To assess beam quality further, the radiated field was compared with the ideal fundamental Gaussian mode (TEM_{00}). This comparison was quantified using two widely adopted correlation metrics: the scalar correlation

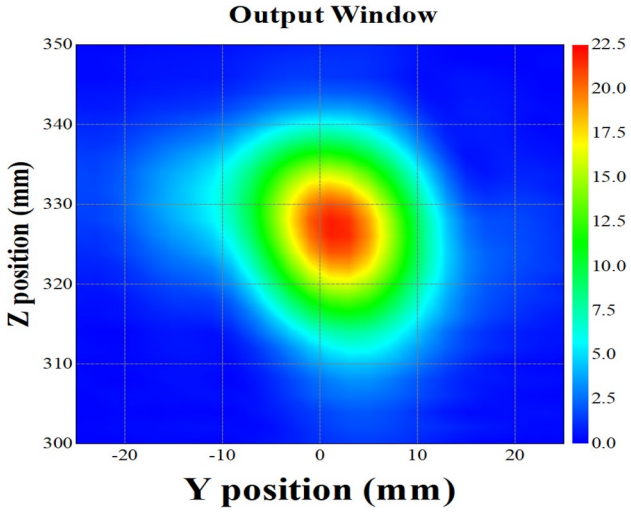

Fig. 8. Electric Field intensity distribution at the output window, as simulated in FEKO.

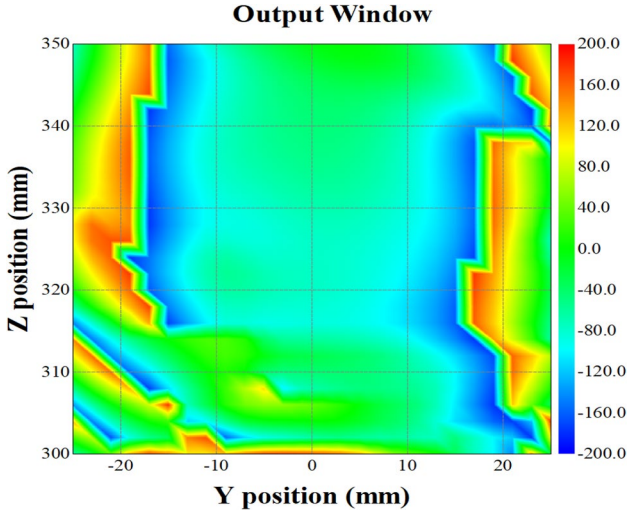

Fig. 9. Phase distribution at the output window, as simulated in FEKO.

coefficient η_s, which evaluates amplitude matching, and the vector correlation coefficient η_v, which incorporates both amplitude and phase alignment. The scalar correlation coefficient η_s is expressed as[23]:

$$\eta_s = \frac{\int_s |u_i|.|u_g| ds}{\sqrt{\int_s |u_i|^2.ds \int_s |u_g|^2.ds}} \tag{12}$$

Similarly, the vector correlation coefficient η_v is given by[23]:

$$\eta_v = \frac{\int_s |u_i|.|u_g| e^{j(\phi_i - \phi_g)ds} . \int_s |u_i|.|u_g| e^{j(\phi_g - \phi_i)ds}}{\sqrt{\int_s |u_i|^2.ds \int_s |u_g|^2.ds}} \tag{13}$$

Here, u_i denotes the numerically computed field, u_g is the ideal Gaussian reference, and ϕ_i and ϕ_g represent their respective phases. A mode purity of 100% corresponds to both coefficients equaling 1, indicating complete suppression of higher-order modes. After optimization of the mirror parameters, the calculated coefficients demonstrate excellent Gaussian purity, with η_s = 99.4% and η_v = 98.6%. These results confirm that the radiated field is overwhelmingly dominated by the fundamental Gaussian mode, with minimal higher-order content.

The power transmission efficiency of the converter system was calculated by comparing the output power across the output window to the injected power of mode $TE_{17,6}$. This efficiency is expressed as $\eta_p = P_{out,field}/P_{in,TE_{17,6}}$, where $P_{in,TE_{17,6}}$ is the injected power of mode $TE_{17,6}$, and $P_{out,field}$ is the total radiated power across the output window plane[31,32]. In our design, this efficiency reached 99%, confirming that

the system transmits power with minimal loss. The Gaussian conversion efficiency is then calculated as $\eta_c = \eta_v \times \eta_p$, yielding a value of approximately 98%, demonstrating the system's high efficiency in maintaining near-ideal Gaussian beam characteristics.[33–35]

In addition to the detailed analysis of the dual-direction perturbation launcher, a comparison with conventional launcher designs near 105 GHz is essential for context. Table 1 summarizes representative launcher designs, highlighting key differences in dimensions and performance metrics. Notably, designs reported in[11,24] for $TE_{17,6}$ launchers at 105 GHz show lengths ranging from 168–170 mm with cut lengths around 40–43 mm, achieving Gaussian content between 95% and 99%. These designs operate at the same frequency and mode as our dual-direction perturbation launcher, providing a direct comparison. In contrast, our dual-direction perturbation launcher achieves the same mode at the same frequency but with a significantly more compact design only 85 mm in total length (cut length of 20 mm, 23.5%) while maintaining 99.4% scalar and 98.6% vector Gaussian content with 98.0% efficiency. This comparison demonstrates the significant advancements made in launcher compactness, mode purity, and overall performance, validating the effectiveness of our dual-direction perturbation method. The remaining designs listed in Table 1 offer additional context, illustrating that conventional launchers typically have lengths ranging from 150–183 mm with cut lengths between 40–68 mm. These designs are tailored for various configurations, with inherent trade-offs in size, Gaussian content, and mode purity. This comparison further emphasizes the advancements made in our work, resulting in a more compact and higher-purity launcher.

Further validation of our approach was done by comparing it with a conventional single-direction perturbation of the same amplitude ($\delta_1 = \delta_2 = +0.172$ mm). In the conventional case, a launcher length of approximately 130 mm was required to achieve mode conversion, but the Gaussian beam quality at the launcher cut was significantly degraded. By contrast, the dual-direction perturbation method reduced the required length to 85 mm while maintaining high mode purity and a shorter cut length. This confirms that our approach offers a more compact and efficient design for beam generation compared to conventional methods.

Conclusion

This study presents the development of a compact quasi-optical mode converter (QOMC) based on the Denisov launcher design, enabling efficient conversion of the $TE_{17,6}$ mode at 105 GHz into a high-purity Gaussian beam. The converter features an optimized dimpled-wall launcher that reduces the length to 85 mm, achieving minimal loss while preserving high mode purity. A novel dual-direction perturbation technique was employed, providing enhanced control over field shaping and enabling further length reduction without compromising performance. Precise mode conversion is further supported by a three-mirror system comprising a quasi-elliptical, elliptical, and parabolic mirror, which ensures accurate beam shaping and phase correction. The launcher design was guided by coupled-mode theory, with structural parameters optimized to enable smooth mode transformation along the waveguide. Parametric analysis was conducted in MATLAB, and electromagnetic field distributions were validated through FEKO simulations. This integrated approach offered detailed insight into field behavior and confirmed the effectiveness of the optimized design, ensuring high mode purity and efficient conversion within a compact configuration. The results validate the design's capability to achieve precise mode conversion and maintain high output quality while minimizing overall system size. This work provides valuable insights into the design of compact QOMCs for 105 GHz high-power millimeter-wave applications, providing a compact and highly efficient solution for advanced gyrotron systems. The proposed design framework is versatile and can be extended to other high-order modes, frequency ranges, and broader millimeter-wave and terahertz applications.

Data availability

The data analyzed during the current study are available from the corresponding author on reasonable request.

Code availability

The code used for the analyses in this study is available from the corresponding author upon request.

Received: 16 April 2025; Accepted: 10 September 2025
Published online: 21 October 2025

References

1. Bogdashov, A. et al. High-efficient mode converter for iter gyrotron. *Int. J. Infrared Millimeter Waves* **26**, 771–785. https://doi.org/10.1007/s10762-005-5651-8 (2005).
2. Denisov, G. G., Litvak, A. G., Zapevalov, V. E., Myasnikov, V. E. & Tai, E. M. Development in russia of high-power gyrotrons for fusion. *Nucl. Fusion* **48**, 054007. https://doi.org/10.1088/0029-5515/48/5/054007 (2008).
3. Glyavin, M. Y. et al. THz Gyrotrons: Status and Possible Optimizations. *Int. J. Terahertz Sci. Technol.* **5**, 67–77. https://doi.org/10.11906/TST.067-077.2012.06.06 (2012).
4. Kumar, N., Singh, U., Singh, T. P., Sharma, A. K. & Sinha, A. K. A review on the applications of high power, high frequency microwave source: Gyrotron. *J. Fusion Energy* **30**, 257–276. https://doi.org/10.1007/s10894-010-9373-0 (2011).
5. Thumm, M. K. Recent developments on high-power gyrotrons-introduction to this special issue. *J. Infrared Millim Terahertz Waves* **32**, 241–252. https://doi.org/10.1007/s10762-010-9754-5 (2011).
6. Denisov, G. et al. 110 ghz gyrotron with a built-in high-efficiency converter. *Int. J. Electron.* **72**, 1079–1091. https://doi.org/10.1080/00207219208925634 (1992).
7. Rock, B. Y. & Fliflet, A. W. Analysis and design of a quasi-optical mode converter for a 1-kw, 550-ghz, $TE_{15,2}$-mode gyrotron. *IEEE Trans. Terahertz Sci. Technol.* **3**, 641–648. https://doi.org/10.1109/TTHZ.2013.2276117 (2013).
8. Bogdashov, A. & Denisov, G. Asymptotic theory of high-efficiency converters of higher-order waveguide modes into eigenwaves of open mirror lines. *Radiophys. Quantum Electron.* **47**, 283–296. https://doi.org/10.1023/B:RAQE.0000047649.17664.6e (2004).
9. Prinz, H. O., Arnold, A., Dammertz, G. & Thumm, M. Analysis of a $te_{22,6}$ 118-ghz quasi-optical mode converter. *IEEE Trans. Microw. Theory Tech.* **55**, 1697–1703. https://doi.org/10.1109/TMTT.2007.902779 (2007).

10. Thumm, M. & Kasparek, W. Passive high-power microwave components. *IEEE Trans. Plasma Sci.* **30**, 755–786. https://doi.org/10.1109/TPS.2002.801653 (2002).
11. Prinz, O. et al. Highly efficient quasi-optical mode converter for a multifrequency high-power gyrotron. *IEEE Trans. Electron Devices* **56**, 828–834. https://doi.org/10.1109/TED.2009.2015819 (2009).
12. Tax, D. S., Choi, E.-M., Mastovsky, I., Thumm, M. & Temkin, R. J. Experimental results on a 1.5 mw, 110 ghz gyrotron with a smooth mirror mode converter. *J. Infrared Millim Terahertz Waves* **32**, 358–370. https://doi.org/10.1007/s10762-010-9720-2 (2011).
13. Zapevalov, V. & Moiseev, M. Influence of aftercavity interaction on gyrotron efficiency. *Radiophys. Quantum Electron.* **47**, 520–527. https://doi.org/10.1023/B:RAQE.0000047243.18212.1d (2004).
14. Sharif, H., Jamil, M. H. & He, W. Optimized quasi-optical mode converter for te33,12 in 210 ghz gyrotron. *Micromachines* **16**, 308. https://doi.org/10.3390/mi16030308 (2025).
15. Choi, E. M., Shapiro, M. A., Sirigiri, J. R. & Temkin, R. J. Experimental observation of the effect of aftercavity interaction in a depressed collector gyrotron oscillator. *Physics of Plasmas* **14**, 093302. https://doi.org/10.1063/1.2776911 (2007).
16. Möbius, A. Conditions to achieve stable propagation of a gaussian-beam-like mode mixture in a deformed waveguide. In *17th International Conference on Infrared and Millimeter Waves*, vol. 1929 of *Proc. SPIE*, 19290J (SPIE, 1992). https://doi.org/10.1117/12.2298136.
17. Pretterebner, J. Improvement of quasi-optical mode converters by launching an appropriate mixture of modes. In *17th International Conference on Infrared and Millimeter Waves*, vol. 1929 of *Proc. SPIE*, 19290M (SPIE, 1992). https://doi.org/10.1117/12.2298139.
18. Thumm, M. et al. Frequency step-tunable (114–170 ghz) megawatt gyrotrons for plasma physics applications. *Fusion Eng. Des.* **53**, 407–421. https://doi.org/10.1016/S0920-3796(00)00519-6 (2001).
19. Denisov, G. G. et al. 110 ghz gyrotron with a built-in high-efficiency converter. *Int. J. Electron.* **72**, 1079–1091. https://doi.org/10.1080/00207219208925634 (1992).
20. Sakamoto, K. et al. Development of high power 170 GHz gyrotron for ITER. In *Conference Digest of the 2004 Joint 29th International Conference on Infrared and Millimeter Waves and 12th International Conference on Terahertz Electronics*, 109–110 (2004). https://doi.org/10.1109/ICIMW.2004.1421977.
21. Albertia, S. et al. European high-power CW gyrotron development for ECRH systems. *Fusion Eng. Des.* **53**, 387–397. https://doi.org/10.1016/S0920-3796(00)00514-7 (2001).
22. Sharif, H., Jamil, M. H., He, W. & Abbas, N. S. Design of quasi-optical te17,6 mode converter for high-power 170-ghz gyrotrons. *IEEE Trans. Plasma Sci.* **53**, 834–841. https://doi.org/10.1109/TPS.2025.3541737 (2025).
23. Jin, J. Quasi-optical mode converter for a coaxial cavity gyrotron. *Wissenschaftliche Berichte FZKA* **7264** (2007). https://doi.org/10.5445/IR/270067871.
24. Mondal, D., Yuvaraj, S., Adya, S., Thakur, A. S. & Kartikeyan, M. V. Design studies of quasi-optical mode converter for 105 ghz high-power gyrotron. In *2020 IEEE 21st International Conference on Vacuum Electronics (IVEC)*, 281–282 (IEEE, 2020). https://doi.org/10.1109/IVEC45766.2020.9520522.
25. Huang, Q. et al. Design of a quasi-optical mode converter for a dual-frequency gyrotron. In *2021 46th International Conference on Infrared, Millimeter and Terahertz Waves (IRMMW-THz)*, 1–2 (IEEE, 2021). https://doi.org/10.1109/IRMMW-THz50926.2021.9567254.
26. Yang, X. et al. Investigation of a broadband quasi optical mode converter for a multi-frequency 1 mw gyrotron. In *Infrared and Millimeter Waves, Conference Digest of the 2004 Joint 29th International Conference on and 12th International Conference on Terahertz Electronics*, 485–486 (IEEE, 2004). https://doi.org/10.1109/ICIMW.2004.1422175.
27. Neilson, J. M. Optimization of quasi-optical launchers for multifrequency gyrotrons. *IEEE Trans. Plasma Sci.* **35**, 1743–1746. https://doi.org/10.1109/TPS.2007.908910 (2007).
28. Prinz, O. et al. Quasi-optical mode converter for a multi-frequency d-band gyrotron. In *2007 Joint 32nd International Conference on Infrared and Millimeter Waves and the 15th International Conference on Terahertz Electronics*, 888–889, https://doi.org/10.1109/ICIMW.2007.4516778 (2007).
29. Thumm, M. Modes and mode conversion in microwave devices. In *Generation and Application of High Power Microwaves*, 121–171 (CRC Press, 2020).
30. Jain, R., Kartikeyan, M. V. & Thumm, M. Design studies of a quasi-optical launcher for a 170 ghz, 200–250 kw gyrotron. In *2009 34th International Conference on Infrared, Millimeter, and Terahertz Waves*, 1–2 (IEEE, 2009). https://doi.org/10.1109/ICIMW.2009.5325653.
31. Liu, J. et al. Vector method for synthesis of adapted phase-correcting mirrors for gyrotron output couplers. *IEEE Trans. Plasma Sci.* **41**, 2489–2495. https://doi.org/10.1109/TPS.2013.2276915 (2013).
32. Dong, X., Ming, J. & Ming, B. Asymmetrical mirror optimization for a 140 ghz te22,6 quasi-optical mode converter system. *Chinese Physics B* **26**, 074101. https://doi.org/10.1088/1674-1056/26/7/074101 (2017).
33. Jin, J., Piosczyk, B., Thumm, M., Rzesnicki, T. & Zhang, S. Quasi-optical mode converter/mirror system for a high-power coaxial-cavity gyrotron. *IEEE Trans. Plasma Sci.* **34**, 1508–1515. https://doi.org/10.1109/TPS.2006.877627 (2006).
34. Litvak, A. G., Denisov, G. G. & Glyavin, M. Y. Russian gyrotrons: Achievements and trends. *IEEE J. Microw.* **1**, 260–268. https://doi.org/10.1109/JMW.2020.3030917 (2021).
35. Zhao, G. et al. Design of quasi-optical mode converter for 170-ghz te32,9-mode high-power gyrotron. *IEEE Trans. Plasma Sci.* **47**, 2582–2589. https://doi.org/10.1109/TPS.2019.2908503 (2019).

Acknowledgements

I would like to express my sincere gratitude to Wenlong He for their invaluable guidance and support throughout this research.

Author contributions

Hamid Sharif led the study's conceptualization, designed the simulation, and directed the overall planning and execution of the project. He also drafted the initial version of the manuscript and played a major role in the revisions. Muhammad Haris Jamil and Nazish Saleem Abbas contributed to data visualization, preparing figures and tables. Wenlong He. provided supervision and offered critical insights and guidance throughout the research.

Funding

This work was supported in part by the Shenzhen Science and Technology Program (Grant no. KQTD20200820113046084) and in part by the National Key Research and Development Program of China (Grant no. 2023YFF0719300).

Declarations

Competing interests
The authors declare no competing interests.

Ethics approval and consent to participate
This declaration is not applicable.

Consent for publication
All authors consent to the publication of this manuscript and have approved the final version submitted to the journal.

Additional information
Correspondence and requests for materials should be addressed to H.S. or W.H.

Reprints and permissions information is available at www.nature.com/reprints.

Publisher's note Springer Nature remains neutral with regard to jurisdictional claims in published maps and institutional affiliations.